Structure, dynamics, and trace gases variability within the Asian summer monsoon anticyclone in extreme El Niño of 2015-16

Saginela Ravindra Babu[1] [*], Madineni Venkat Ratnam[2], Ghouse Basha[2], Shantanu Kumar Pani[1] and Neng-Huei Lin[1,3*]

[1]Department of Atmospheric Sciences, National Central University, Taoyuan 32001, Taiwan

[2]National Atmospheric Research Laboratory, Gadanki 517112, India.

[3]Center for Environmental Monitoring and Technology, National Central University, Taoyuan 32001, Taiwan

*Correspondence to: S.Ravindra Babu (baburavindra595@gmail.com) and N.-H. Lin (nhlin@cc.ncu.edu.tw)

Abstract: A weak El Niño during 2014-15 boreal winter was developed as a strong boreal summer event in 2015 which continued and even enhanced during the following winter. In this work, the detailed changes in the structure, dynamics and trace gases within the Asian summer monsoon anticyclone (ASMA) during extreme El Niño of 2015-16 is delineated by using Aura Microwave Limb Sounder (MLS) measurements, COSMIC Radio Occultation (RO) temperature, and NCEP reanalysis products. Our analysis concentrates only on the summer months of July and August 2015 when Nino 3.4 index started to exceed 1.5 values. The results show that the ASMA structure was quite different in summer 2015 as compared to the long-term (2005-2014) mean. In July, the spatial extension of the ASMA shows larger than the long-term mean in all the regions except over northeastern Asia, where, it exhibits a strong southward shift in its position. The ASMA splits into two and western Pacific mode is evident in August. Interestingly, the subtropical westerly jet (STJ) shifted southward from its normal position over northeastern Asia as resulted mid-latitude air moved southward in 2015. Intense Rossby wave breaking events along with STJ are also found in July 2015. Due to these dynamical changes in the ASMA, pronounced changes in the ASMA tracers are noticed in 2015 compared to the long-term mean. A 30% (20%) decrease in carbon

26   monoxide (water vapor) at 100 hPa is observed in July over most of the ASMA region, whereas

27   in August the drop is strongly concentrated in the edges of the ASMA. Prominent increase of O_3

28   (>40%) at 100 hPa is clearly evident within the ASMA in July, whereas in August the increase is

29   strongly located (even at 121 hPa) over the western edges of the ASMA. Further, the temperature

30   around the tropopause shows significant positive anomalies (~5K) within the ASMA in 2015. The

31   present results clearly reveal the El Niño induced dynamical changes caused significant changes

32   in the trace gases within the ASMA in summer 2015.

33   **Keywords:** Trace gases, El Niño, Asian summer monsoon anticyclone, tropopause

34   **1. Introduction**

35   The Asian summer monsoon anticyclone (ASMA) is a distinct circulation system in the upper

36   troposphere and lower stratosphere (UTLS) during northern hemisphere boreal summer, centered

37   at ~25ºN and extending roughly between 15ºN to 40ºN (Park et al., 2004; Randel et al., 2010). It

38   is encircled by the subtropical westerly jet stream to the north and by the equatorial easterly jet to

39   the south (Randel and Park, 2006). It is well recognized that the ASMA circulation is a prominent

40   transport pathway for troposphere pollutants to enter the stratosphere (Randel et al., 2010).

41   Previous studies have concluded that deep convection during summer monsoon can effectively

42   transport the pollutants, aerosols and tropospheric tracers from the boundary layer into the UTLS

43   region (Vogel et al., 2016; Santee et al., 2017). These transported pollutants, tracers and aerosols

44   become confined in the ASMA and, consequently, affect the trace gas composition in the UTLS

45   region (Randel et al., 2010; Solomon et al., 2010; Riese et al., 2012; Hossaini et al., 2015). It is

46   clearly evident from the previous studies that the ASMA has a higher concentrations of

47   tropospheric tracers such as carbon monoxide (CO), hydrogen cyanide (HCN) and Methane (CH_4)

48   and lower concentrations of stratospheric tracers including Ozone (O_3) and nitric acid (HNO_3)

49   (Park et al., 2004; Li et al., 2005; Park et al., 2008; Randel et al., 2010; Vernier et al., 2015; Yan

50   and Bian, 2015; Yu et al., 2017; Santee et al., 2017; Vernier et al., 2018). The comprehensive study

51   on the climatological composition within the ASMA can be found in Santee et al. (2017). The ASM

52   convection and orographic lifting are the primary mechanisms for the higher concentrations of the

53   tropospheric tracers in the ASMA (Li et al., 2005; Park et al., 2009; Santee et al., 2017). Apart

54   from these trace gases a strong persistent tropopause-level aerosol layer called as 'Asian

55   Tropopause Aerosol Layer' (ATAL) also existed between 12 to 18 km within the ASMA and it was

56   first detected from the CALIPSO measurements (Vernier et al., 2011).

57   Similarly, higher concentrations of water vapor (WV) within the ASMA during the summer

58   monsoon is well documented in the literature (Gettelman et al., 2004; Park et al., 2007; Randel et

59   al., 2010; Bian et al., 2012; Xu et al., 2014; Jiang et al., 2015; Das and Suneeth, 2020). It is well

60   known that most of the WV enters the stratosphere through the tropical tropopause (Fueglistaler

61   et al., 2009) and the temperature presented at the tropical tropopause strongly controls the WV

62   entering the lower stratosphere (LS). It is also well documented that several processes such as

63   convection, strength of the Brewer-Dobson circulation, El Niño–Southern Oscillation (ENSO) and

64   Quasi-Biennial Oscillation (QBO) are responsible for the WV transport to the UTLS region

65   (Holton et al., 1995; Dessler et al., 2014; Jiang et al., 2015). Other factors such as gravity waves

66   and horizontal advection can also influence the WV transport in the UTLS region. For example,

67   Khan and Jin (2016), studied the effect of gravity waves on the tropopause and WV over Tibetan

68   Plateau and reported that the gravity wave is the source for the WV transport from the lower to

69   higher altitudes. Recently, Das and Suneeth (2020) reported about the distributions of WV in the

70   UTLS over the ASMA during summer using 13 years of Aura Microwave Limb Sounder

71   observations. They concluded that WV in the UTLS region inside the central part of ASMA is

72 mostly controlled by horizontal advection and very less from the local process and tropopause

73 temperature in both summer and winter.

74   Convection during the summer monsoon is one of the major sources to transport the boundary

75 layer pollutants into the UTLS region (Randel et al., 2010). It is well established fact that the ENSO

76 has a strong influence on convection and circulation changes over the Asian monsoon region

77 (Kumar et al., 1999; Wang et al., 2015; Gadgil and Francis, 2016). Enhanced (suppressed)

78 convection over the Asian monsoon region generally observed in the cold phase of ENSO (warm

79 phase of ENSO) known as La Niña (El Niño). Few studies have existed to date on the impact of

80 ENSO on the ASMA trace gas composition changes and its dynamical changes. For example, Yan

81 et al. (2018) reported the influence of ENSO on the ASMA with a major focus on how the ENSO

82 winter signal propagates into the following seasons. They showed the weaker O_3 transport into the

83 tropics during the onset of the ASMA after boreal winter El Niño events, but the difference between

84 El Niño and La Niña composites becomes insignificant in the summer. In another study, Tweedy

85 et al. (2018) demonstrated the impact of boreal summer ENSO events on O_3 composition within

86 the ASMA in different phases of ENSO events. They reported that the ASMA forms earlier and

87 stronger in the La Niña period that leads to greater equatorward transport of O_3-rich air from the

88 extra-tropics into the northern tropics than during El Niño periods. Recently, Fadnavis et al. (2019)

89 reported higher concentrations of aerosol layers observed in the ATAL region during the El Niño

90 period over the northern part of South Asia. However, the above- mentioned studies are mainly

91 focused on changes in the ASMA with respect to ENSO on seasonal scales or mature stage of

92 monsoon (combined mean of July and August).

93   Based on the above-mentioned studies, it can be concluded that the ENSO also has a strong

94 influence on the ASMA structure and its composition. The recent 2015-16 El Niño event was

95   recorded as an extreme and long-lasting event in the 21st century (Huang et al., 2016; Avery et al.,

96   2017). It was started as a weak El Niño during 2014-15 boreal winter and it developed as a strong

97   boreal summer El Niño event in 2015 (Tweedy et al., 2018). Further, this strong boreal summer

98   event was continued and significantly enhanced until the boreal winter of 2015-16. In this event,

99   several unusual changes occurred in the tropical UTLS region including, the strong enhancement

100   in the lower stratosphere WV (higher positive tropopause temperature anomalies) over Southeast

101   Asia and western Pacific regions (Avery et al., 2017) and anomalous distribution of trace gases in

102   the UTLS region (Diallo et al., 2018; Ravindra Babu et al., 2019a). Similar way, the response of

103   different trace gases (O_3, HCl, WV) to the disrupted 2015–2016 quasi-biennial oscillation (QBO)

104   associated with 2015-16 El Niño event is also reported by Tweedy et al. (2017). Dunkerton (2016),

105   discussed the possible role of unusual warm ENSO event in 2015-2016 to the QBO disruption by

106   triggering the extratropical planetary waves. Therefore, in the present study, we investigated the

107   detailed changes observed in the ASMA 2015 particularly by focusing on the structure, dynamics

108   and trace gases variability within the ASMA in July and August 2015 by using satellite

109   observations and reanalysis products. The present research article is organized as follows.

110   Database and methodology adopted in this study are discussed in Section 2. The results and

111   discussions are illustrated in Section 3. Finally, the summary and conclusions obtained from the

112   present study are summarized in Section 4.

113   **2. Database and Methodology**

114   **2.1. Microwave Limb Sounder (MLS) measurements**

115   In the present study, version 4.2 Aura MLS measurements of CO, O_3 and WV are utilized.

116   The MLS data of July and August months in each year from 2005 to 2015 period are considered.

117   The vertical resolution for CO is in the range 3.5–5 km from the upper troposphere to the lower

118 mesosphere and the useful range is 215–0.0046 hPa. The horizontal resolution for CO is about 460

119 km at 100 hPa and 690 km at 215 hPa. For WV, the vertical resolution is in the range of 2.0 to 3.7

120 km from 316 to 0.22 hPa and the along-track horizontal resolution varies from 210 to 360 km for

121 pressure greater than 4.6 hPa. For O_3, the vertical resolution is ~2.5 km and the along-track

122 horizontal resolution varies between 300 and 450 km. The precision (systematic uncertainty) for

123 WV is ~ 10-40% (~10-25%), for O_3 is ~0.02–0.04 (~0.02–0.05) ppmv and for CO, it is ~ 19 ppbv

124 (30%), respectively. More details about the MLS version 4 level 2 data can be found in Livesey et

125 al. (2018).

126 **2.2. COSMIC Radio Occultation measurements**

127 To see the changes in the tropopause temperature and height within the ASMA, we used high-

128 resolution, post-processed products of level 2 dry temperature profiles obtained from Constellation

129 Observing System for Meteorology, Ionosphere, and Climate (COSMIC) Radio Occultation (RO).

130 Each month of July and August from 2006 to 2015 are considered. The data is downloaded from

131 the COSMIC Data Analysis and Archival Center (CDAAC) website. We used 200 m vertical

132 resolution temperature profiles in the study. Details of the temperature retrieval from the bending

133 angle and refractivity profiles obtained from the RO sounding are presented well in the literature

134 (Kursinski et al. 1997; Anthes et al. 2008). The COSMIC temperature have a precision of 0.1%

135 between 8 and 25 km (Kishore et al. 2009; Kim and Son, 2012). The temperature accuracy in the

136 UTLS is better than 0.5 K for individual profiles and ~0.1 K for averaged profiles (Hajj et al.

137 2004). It is noted that for individual RO temperature profiles, the observational uncertainty

138 estimate is 0.7 K in the tropopause region, slightly decreasing into the troposphere and gradually

139 increasing into the stratosphere (Scherllin-Pirscher et al., 2011a). For monthly zonal-averaged

140 temperature fields, the total uncertainty estimate is smaller than 0.15 K in the UTLS (Scherllin-

141 Pirscher et al., 2011b). Overall, the uncertainties of RO climatological fields are small compared

142 to any other UTLS observing system for thermodynamic atmospheric variables. Note that these

143 data are compared with a variety of techniques including GPS radiosonde data and observed good

144 correlation particularly in the UTLS region (Rao et al. 2009; Kishore et al. 2009). The COSMIC

145 RO profiles have been widely used for studying the tropopause changes and its variabilities (Kim

146 and Son, 2012; RavindraBabu et al. 2015; RavindraBabu and Liou, 2021).

147 **2.3. National Centers for Environmental Prediction (NCEP) Reanalysis data**

148 We also utilized monthly mean Geopotential height (GPH) and wind vectors (zonal and

149 meridional wind speed) from the NCEP-DOE Reanalysis 2 (Kanamitsu et al.,2002), covering the

150 same time period as the MLS observations (2005-2015). NCEP-DOE Reanalysis 2 is an improved

151 version of the NCEP Reanalysis I model that fixed errors and updated parametrizations of physical

152 processes. The horizontal resolution of NCEP-DOE Reanalysis 2is $2.5° \times 2.5°$, respectively.

153 Apart from the above-mentioned data sets, we also used European Centre for Medium-Range

154 Weather Forecasts (ECMWF) interim reanalysis potential vorticity (PV) data particularly at 350K

155 isentropic surface in July and August 2015 (ERA-Interim; Uppala et al., 2005; Dee et al., 2011).

156 **2.5. Methodology**

157 Daily available MLS profiles of O_3, CO, and WV in each month are constructed and gridded

158 by averaging the profiles inside bins with a resolution of 5° latitude $\times$ 5° longitudes. The following

159 equation is used to estimate the relative change in percentage.

160 Relative change in percentage $= \left(\frac{x_{i-\bar{x}}}{\bar{x}}\right) \times 100$ (1)

161 where x_i represents the monthly mean of July/August in 2015, and $\bar{x}$ is the corresponding monthly

162 long-term mean which is calculated by using the data from 2005 to 2014.

163 **3. Results and Discussion**

164 It is well reported that the ASMA is highly dynamic in nature with respect to its position and shape.

165 Also it varies at different time scales i.e day-to-day, weekly and monthly scales caused by internal

166 dynamical variability (Randel and Park, 2006; Garny and Randel, 2013; Pan et al., 2016; Nützel

167 et al., 2016; Santee et al., 2017). The intensity and spatial extension of the ASMA are prominent

168 in July and August where the monsoon was in the mature phase (Santee et al., 2017; Basha et al.,

169 2019). It can be noticed that the 2015-16 El Niño event was one of the strongest boreal summer

170 events that occurred in the entire MLS data record (Tweedy et al., 2018). In this event, the Nino

171 3.4 data was exceeded +1.5 in July and +1.8 in August (**Fig. 1**). Therefore, in the present study,

172 we mainly focused on ASMA behavior and trace gases changes within the ASMA on monthly

173 scales particularly in July and August 2015 which represents strong El Niño.
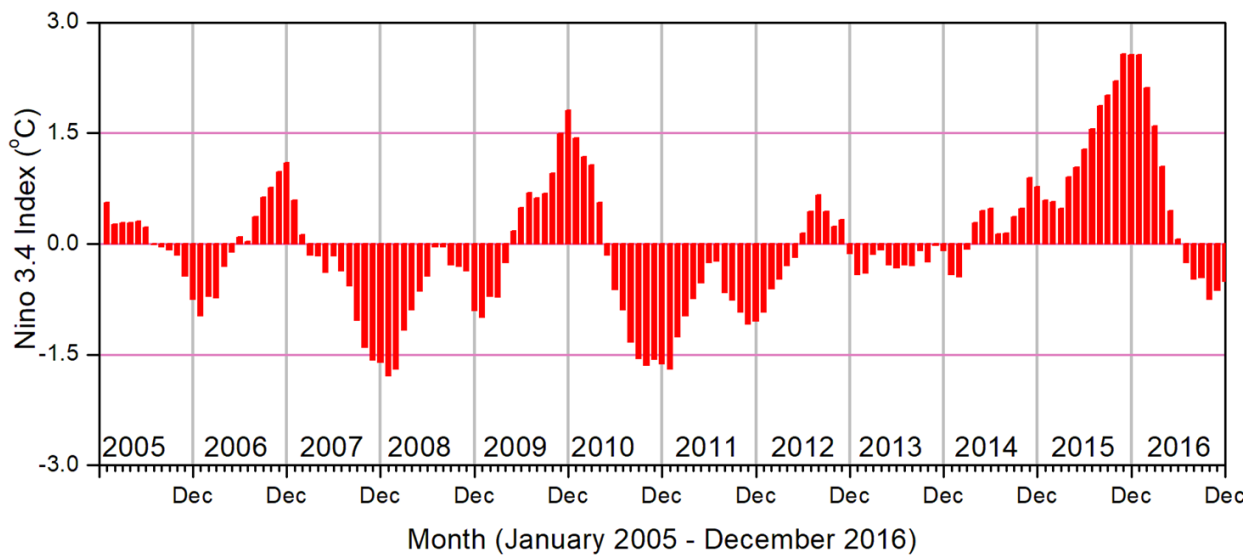
174

175 **Figure 1**. Temporal evolution of observed Niño3.4 Index data from January 2005 to December

176 2016.

177 **3.1. Structure and dynamical changes in ASMA during 2015**

178   In general, the studies looking at monthly or seasonal timescales related to the thermo-

179 dynamical features in the ASMA, the anticyclone region is mostly defined from the simple

180 constant GPH contours at different pressure levels (Randel and Park, 2006; Yan et al., 2011;

181   Bergman et al., 2013; Basha et al., 2019). Previous researchers used different GPH contours at 100

182   hPa to define the anticyclone region. For example, Yan et al. (2011) used 16.7 km, Bergman et al.

183   (2013) used 16.77 km and recently Basha et al. (2019) used 16.75 km GPH contour as the

184   anticyclone region. In a similar manner, we also defined the ASMA region based on NCEP-DOE

185   Reanalysis 2 obtained GPH at 100 hPa and considered the 16.75 km GPH contour as the

186   anticyclone region.
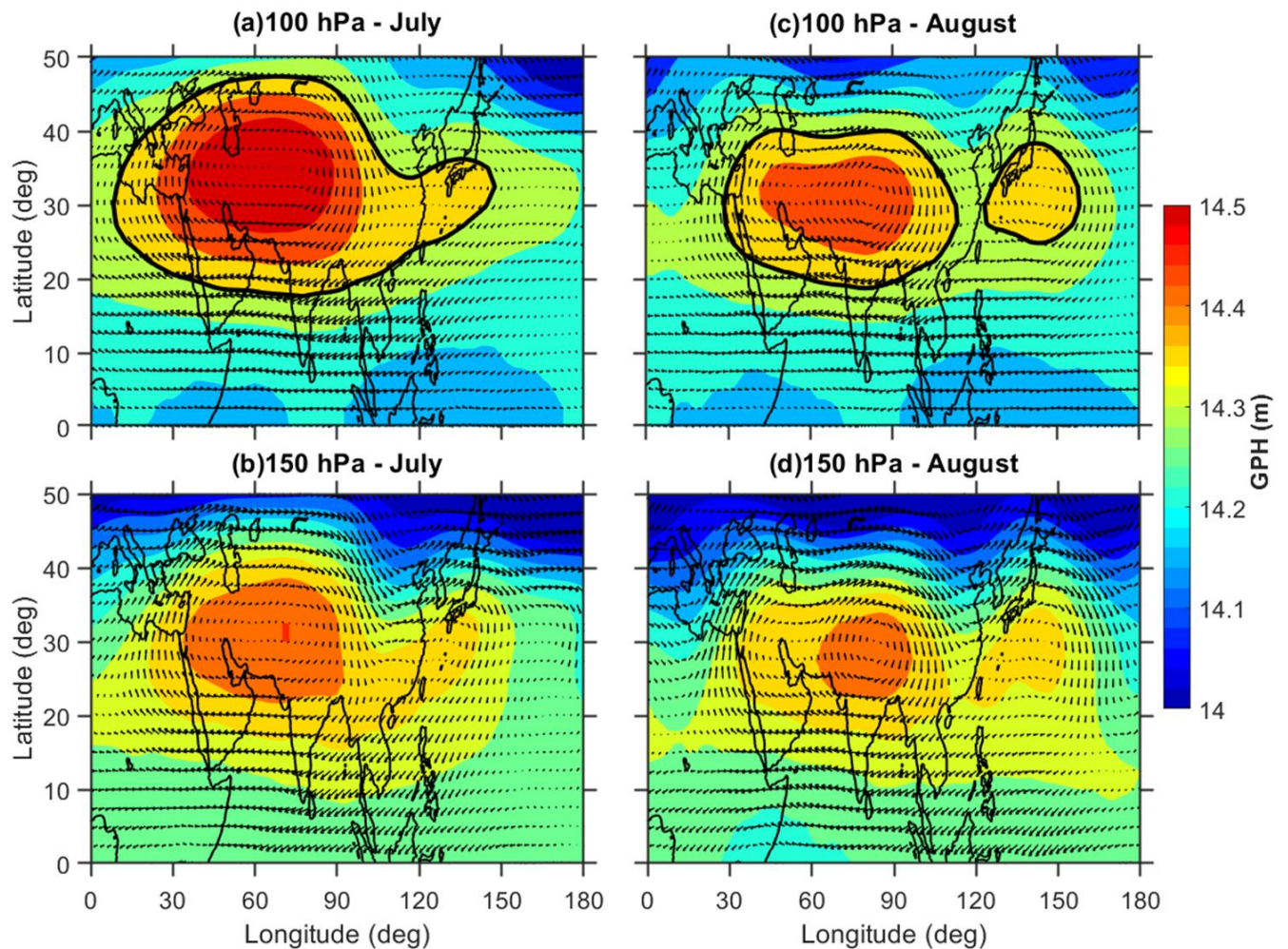
187

188   **Figure 2.** Spatial distribution of geopotential height obtained from NCEP-DOE Reanalysis 2 data

189   during July 2015 (a) at 100 hPa and (b) 150 hPa superimposed with wind vectors at the respective

190   corresponding levels. Subplots of (c) and (d) are the same as (a) and (b) but for the month of

191   August. The black color solid contour lines represent the ASMA region at 100 hPa (16.75 km GPH

192   contour).

193   The spatial distribution of GPH at 100 hPa and 150 hPa for the month of July (August) is

194   shown in **Fig. 2a and 2b (Fig. 2c and 2d).** The corresponding monthly mean winds at respective

195   pressure levels are also shown in **Fig.2**, respectively. The black solid line represents the ASMA

196   region at 100 hPa based on 16.75 km GPH contour. The GPH distribution in **Fig. 2** shows clear

197   distinct variability in the ASMA spatial structure between July and August at both pressure levels.

198   For example, at 100 hPa, the maximum GPH center was located over western side in July whereas

199   it was located over near to the Tibetan region in August. Interestingly the ASMA itself separated

200   into two anticyclones (16.75 km GPH contour black solid line in the figure) in August compare to

201   July. The center of the small anticyclone was located over the Northwestern Pacific near 140ºE

202   with the closed circulation indicated by the wind arrows.

203
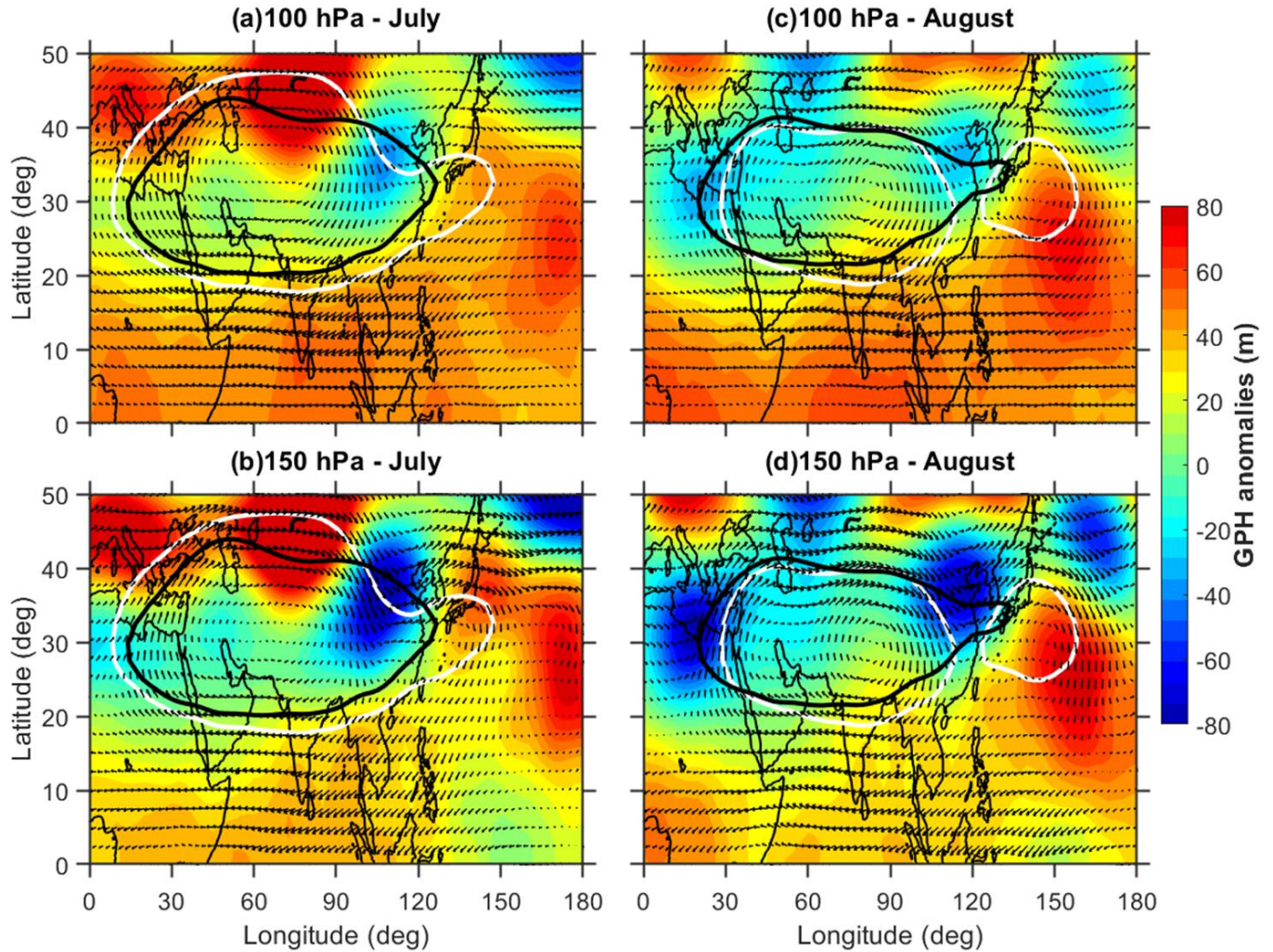
Figure 3. Spatial distribution of geopotential height anomalies obtained from NCEP-DOE Reanalysis 2 data during July 2015 (a) at 100 hPa and (b) 150 hPa superimposed with wind vectors at the respective corresponding levels. Subplots of (c) and (d) same as (a) and (b) but for the month of August. The white color solid contour lines represent the ASMA region at 100 hPa (16.75 km GPH contour) observed in 2015 whereas the black color line represents the mean of 2005-2014.

Further, we compared the ASMA structure in 2015 with referenced long-term mean. For this, we obtained the GPH anomalies by subtracting the background long-term mean (2005-2014) from 2015. **Figure 3** shows the latitude-longitudinal distribution of GPH anomalies (color shaded) along with wind vectors depicting circulation pattern at 100 hPa as well as at150 hPa during July and August. The white (black) color contour represents 16.75 km GPH at 100 hPa for the

215   corresponding month in 2015 (long-term mean). The GPH anomalies at both pressure levels show

216   quite different features in July and August. A clear wave-like structures can be observed from the

217   GPH anomalies. In July, the GPH anomalies exhibit strong negative maxima over 25-40°N, 90-

218   120°E and positive maxima over 40-50°N, 60-80°E regions. The 16.75 km GPH contour lines in

219   the ASMA region exhibits higher extension in all the directions except over the northeastern edges

220   of the ASMA in July compared to the long-term mean. At the same location (northeastern edges),

221   the ASMA exhibits a pronounced southward extension in July. Distinct features of GPH anomalies

222   are noticed in August as compared to July. In August, the strong negative GPH anomalies are

223   situated over the west and north-eastern edges of the ASMA.

224   It is well known that the subtropical westerly jet is an important characteristic feature of

225   the ASMA (Ramaswamy 1958), and thus its changes during 2015 are also investigated. As the

226   peak intensity of the westerly jet was located at 200 hPa (Chiang et al., 2015), we focused mainly

227   on 200 hPa zonal wind changes in July and August. **Figure 4a and 4c** (**Fig. 4b and 4d**) show the

228   spatial distribution of long-term (2015) monthly mean zonal wind at 200 hPa during July and

229   August. In general, the subtropical westerlies are located near to ~40°N latitude during the mature

230   phase of the monsoon period (Chiang et al., 2015). Compared to long-term mean, a significant

231   weakening of the subtropical westerlies is noticed in 2015. Further, a strong southward shift in the

232   westerlies is observed over the northeastern Asia region. This southward shift is moved even up

233   to 30°N in both months. From zonal wind at 200 hPa (**Fig. 4**) and wind vectors at 100/150 hPa

234   (**Fig. 2**), it is clear that anomalous changes have occurred in the subtropical westerlies over the

235   northeastern parts of the AMSA around 30-40°N, 90-120°E during July and August 2015. The

236   southward shift in the westerlies is strongly associated with the southward extension of the ASMA

237   over the northeastern side of the ASMA (**Fig. 2**). This is strongly supported by the previous

238 findings by Lin and Lu (2005) where they showed the southward extension of the South Asian

239 High could lead to the southward shift of the westerlies.

240
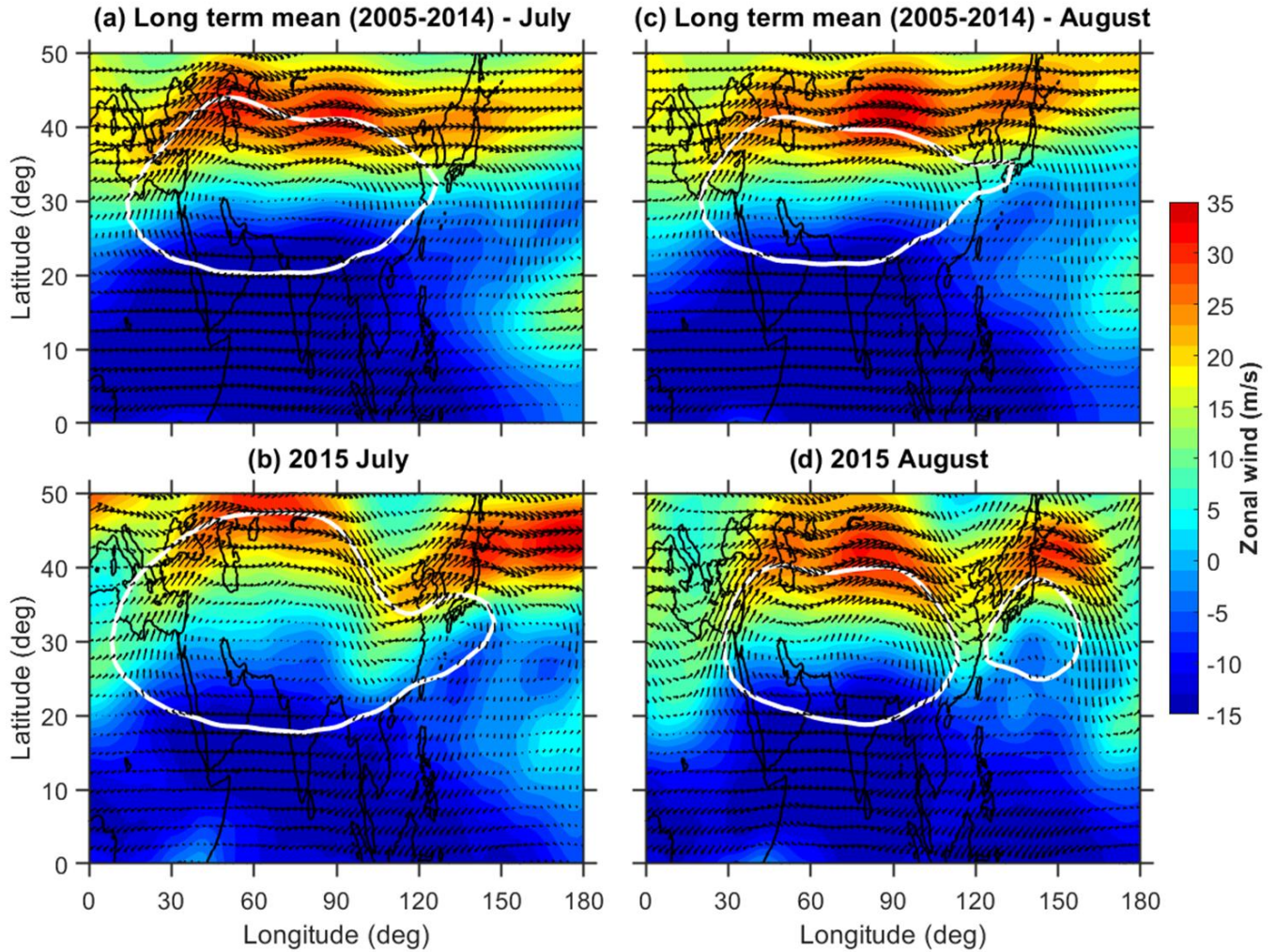
241
242 **Figure 4.** Spatial distribution of monthly mean zonal winds obtained from NCEP-DOE Reanalysis

243 2 data at 200 hPa during July during (a) 2005-2014 (b) 2015 year. Subplots of (c) and (d) same as

244 (a) and (b) but for the month of August. The white color solid contour lines represent the ASMA

245 region at 100 hPa (16.75 km GPH contour).

246   From the GPH and winds observations, it is clear that pronounced changes are evident in

247 the dynamical structure of the ASMA in 2015 and also relatively different features are noticed

248 between July and August months. Interestingly the ASMA itself separated into two anticyclones

249 during August 2015 and the separation exactly coincided with the strong negative GPH anomalies

250 and southward meandering of subtropical westerlies over the northeastern side of the ASMA. The

251 Western Pacific (WP) mode of the anticyclone is visible in August. The split of the anticyclone

252 and the formation of the WP mode are in agreement with previous studies reported by few

253 researchers earlier (e.g. Honomichl and Pan, 2020). The presence of the WP mode may be due to

254 the eastward eddy shedding of the ASMA system in the process of its sub-seasonal zonal

255 oscillation (Honomichl and Pan, 2020) or Rossby wave breaking (RWB) in the subtropical

256 westerly jet (Fadnavis and Chattopadhyay, 2017). Fadnavis and Chattopadhyay (2017) also

257 identified the split of ASMA into two anticyclones: one over Iran and another over the Tibetan

258 region due to the RWB in June 2014 monsoon period. To see any signatures of these RWB in 2015,

259 we further analyzed the RWB through the ERA interim reanalysis potential vorticity (PV) data.

260 Based on previous studies, it is reported that RWBs can be identified from PV distribution at 350

261 K isentropic surface (Samanta et al. 2016; Fadnavis and Chattopadhyay, 2017). We used 350 K

262 isentropic surface PV data in July and August 2015 in the present analysis.

263   **Figure 5a–b** shows the distribution of ERA interim monthly mean PV at the 350 K

264 isentropic surface during July and August 2015. It can be seen that, during July and August 2015,

265 clear RWB signatures evident near 100ºE. It is noted that the equatorial advection of high PV

266 values with a steep gradient and the southward movement of PV from the westerly jet are the basic

267 features of the RBW (Vellore et al., 2016; Samanta et al. 2016). These features are clearly exhibited

268 in **Figure 5** with higher PV values extends up to ~ 30ºN in both months over 100ºE region. The

269 location of this RWB is significantly correlated with a southward meandering of westerlies and

270 strong negative GPH anomalies. However, the observed RWB signatures in both months are from

271 monthly mean PV data. Further, to see the clear signatures of these RWB, we made weekly based

272 analysis for July month. For this we considered 1-7 July as week-1 and 8-14 July as week-2 so on.

273 The weekly mean distribution of 350K isentropic surface PV during July is shown in **Fig. 6**.

274
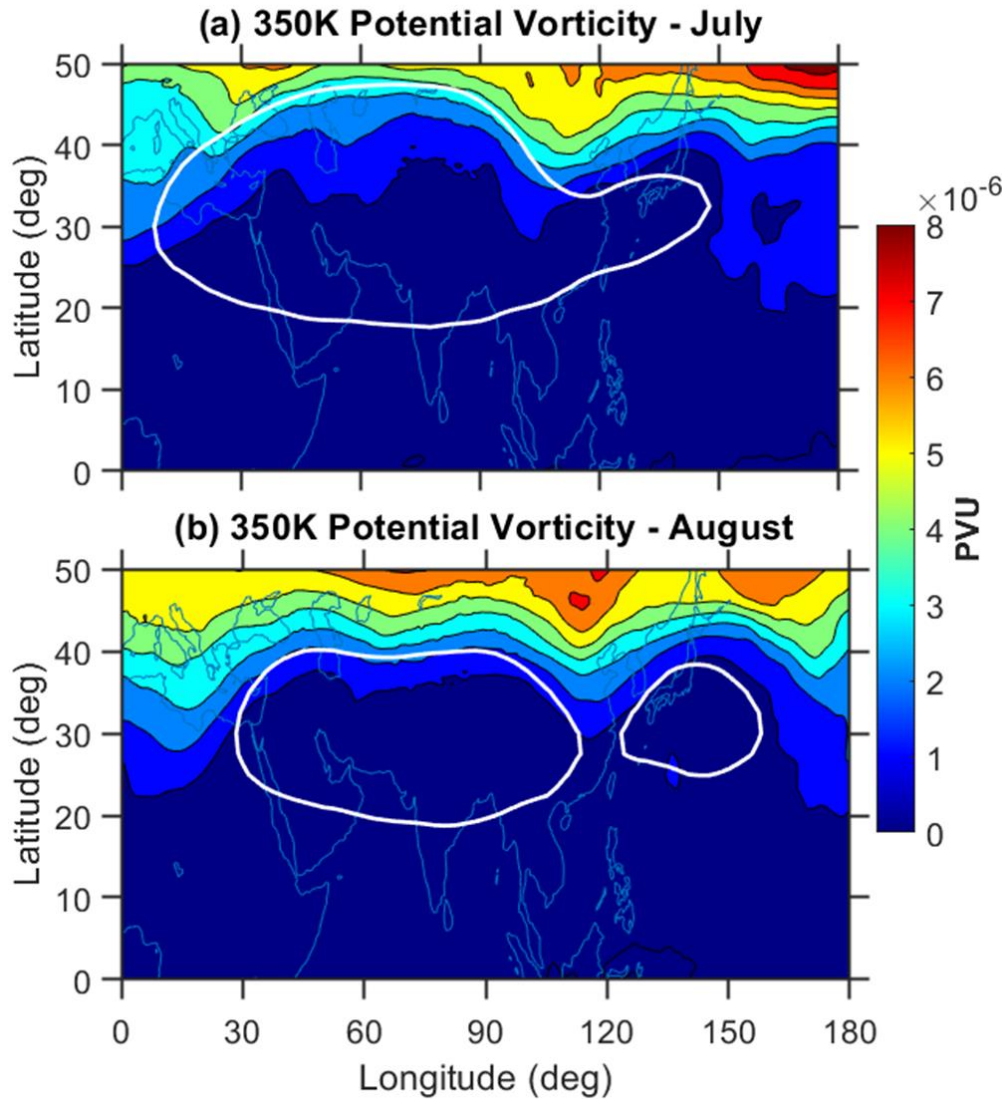
Figure 5. ERA Interim observed spatial distribution of potential vorticity (PV) on a 350 K isentropic surface in PVU (1 PVU = 10^{-6} K m^2 kg^{-1}s^{-1}): (a) monthly mean of July and (b) monthly mean of August 2015. The white color solid contour lines represent the ASMA region at 100 hPa (16.75 km GPH contour).

The magenta colored arrows which are shown in the Fig. 6 represents the RBW events during July 2015. A clear signature of air with high values of PV traverses from extra-tropics to ASMA is evident from Fig.6. At weekly scales, clear RWB signatures are observed over the anticyclone region. For example, in week-1 and week-2, the RWB signatures are evident over the northern

283 region of the ASMA. However, in week-3 and week-4, these RWB signatures are very clear over

284 northeastern Asia even in week-5 (29July-04August), we noticed RWB signatures in PV data

285 (Figure not shown). This clearly shows that The RWB splits the ASMA into two anticyclones: one

286 over the Tibetan region and another over the WP region. It is clear that the equatorward penetration

287 of extra tropical forcing through the subtropical westerly jet has started in July and further

288 amplified by the splitting of the ASMA into two during August.
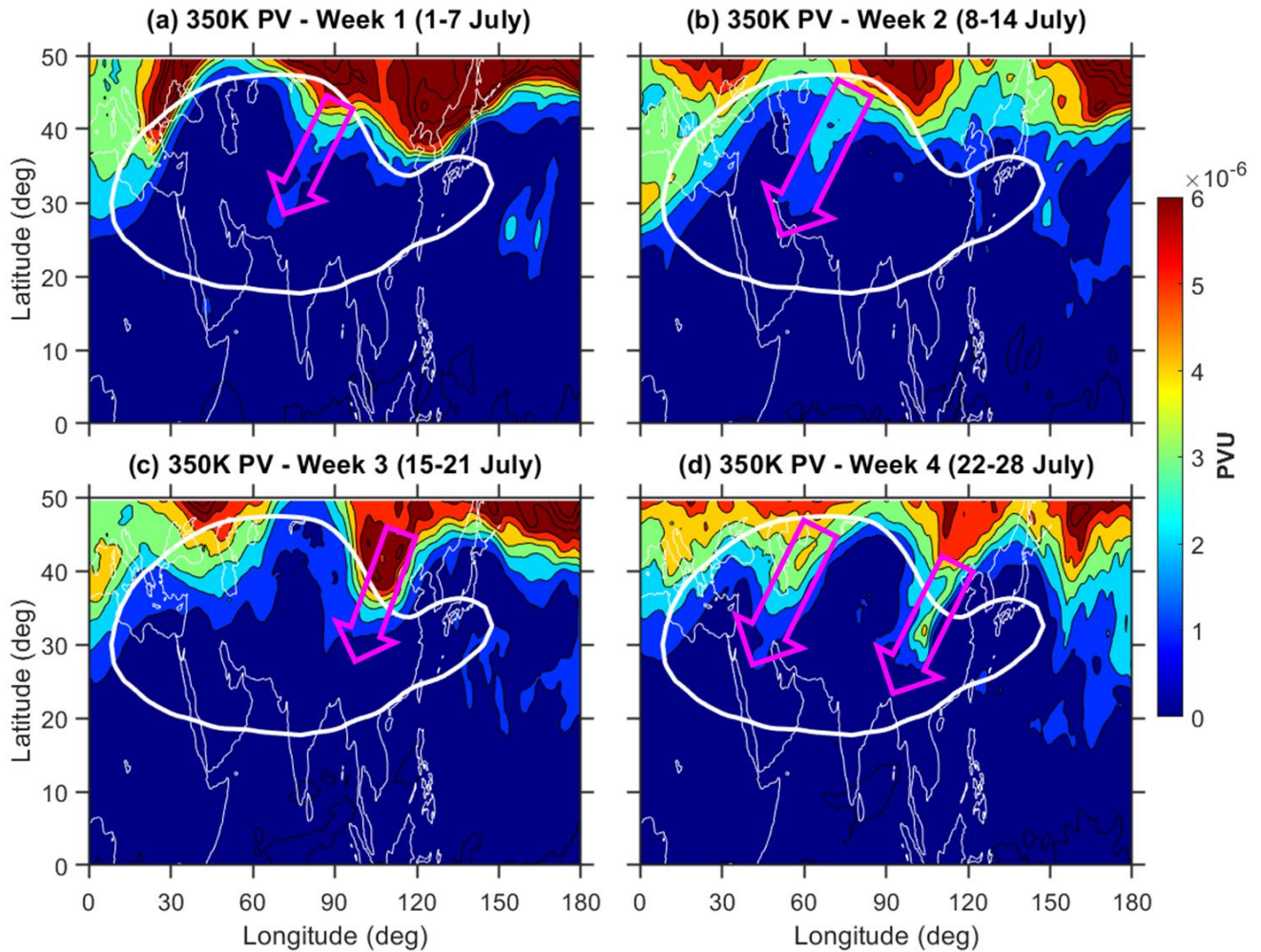
289

290 **Figure 6.** Same as **Figure 5**, but for the weekly distribution of PV in July 2015. Magenta colored

291 arrows indicate the regions of RWB.

292 It is well known that the RWB is an important mechanism for horizontal transport between

293 the extratropical lower stratosphere to the tropical UTLS region. These RWBs can act as an agent

294   for the transport of extratropical stratospheric cold, dry, and O_3-rich air into the ASMA during the

295   summer monsoon. Overall, it is concluded that the combination of the RWBs and strong southward

296   meandering of the subtropical westerly jet in 2015 causes significant dynamical and structural

297   changes in the ASMA. These changes in the ASMA dynamical structure in 2015 can influence the

298   concentrations of the different trace gases within the ASMA. Further, we quantified the changes

299   in O_3, CO and WV concentrations within the ASMA during 2015 caused by the dynamical effects.

300   The changes that occurred in the O_3 and CO, WV, are discussed in the following sections.

3.2. Trace gases anomalies observed within the ASMA in 2015

302   It is well-documented that the ASMA contains low (high) concentrations of stratospheric

303   tracers such as O_3 (tropospheric tracers such as CO, WV and etc.) and higher tropopause height

304   compared to the region outside the ASMA during boreal summer (Park et al., 2007; Randel et al.,

305   2010; Santee et al., 2017; Basha et al., 2019). Differences of the trace gases within and outside of

306   the ASMA are attributed to the strong winds and closed streamlines associated with the ASMA,

307   which act to isolate the air (Randel and Park 2006; Park et al. 2007). To see the changes in the

308   trace gases during 2015, we generated the background long-term mean of CO, O_3, and WV by

309   using 10 years of MLS trace gas data from 2005 to 2014. Here the results are discussed mainly

310   based on the percentage changes relative to the respective long-term monthly mean trace gases

311   using **Equ. 1**.

312
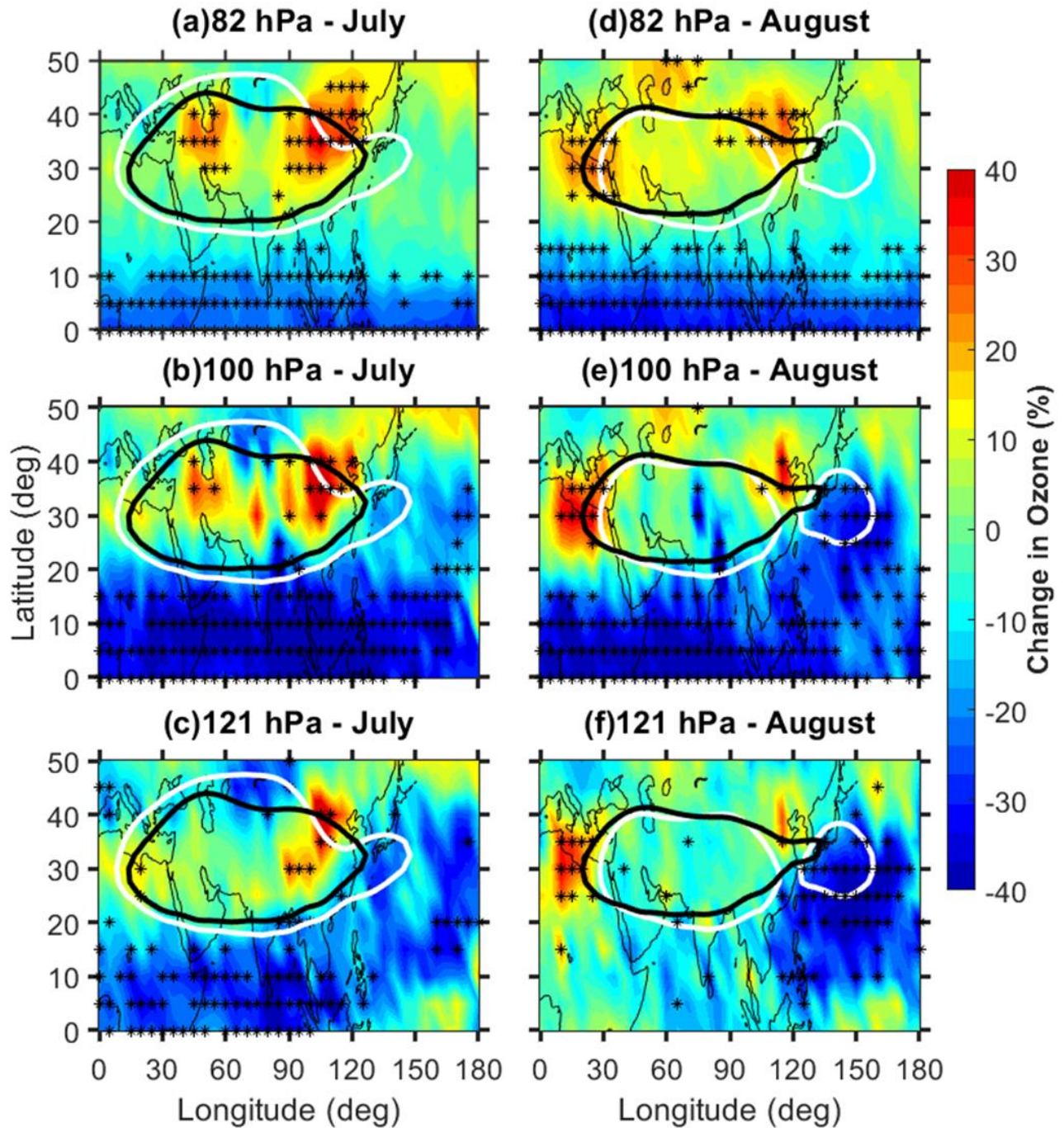
Figure 7. Ozone relative percentage change in July 2015 with respect to background climatological monthly mean observed at (a) 82 hPa, (b) 100 hPa and (c) 121 hPa. Subplots of (d), (e) and (f) same as (a), (b) and (c) but for the month of August. The white (black) color contour represents 16.75 km geopotential height at 100 hPa for the corresponding month in 2015 (mean of 2005-2014). The star symbols (black) shown in figure represent the anomalies greater than the ±2σ standard deviation of long-term mean. The results are obtained from MLS measurements.

320   **Figure 7a-c** (**Fig. 7d-f**) shows the distribution of relative percentage change in the O_3

321   concentrations within the ASMA at 82 hPa, 100 hPa and 121 hPa during July (August) 2015. The

322   anomalies larger than $\pm 2\sigma$ standard deviation of long-term mean are highlighted with star symbols

323   in the respective figures. The spatial distribution of changes in the O_3 (Fig. 7) shows a clear

324   increase in the O_3 mixing ratios (>40%) within the ASMA in 2015. The observed increase within

325   the ASMA is quite distinct between July and August. In July, the O_3 shows a pronounced increase

326   within the ASMA at all the pressure levels. Note that the observed increase was statistically

327   significant with larger than 2σ standard deviation of long-term mean (see the star symbols). This

328   increase is quite significant over the northeastern edges of the ASMA and quite high at 100 hPa

329   compared to 82 hPa and 121 hPa. In August, the O_3 shows quite different features compared to

330   July (Fig. 7d-f). A strong increase in the O_3 is observed over the western and eastern edges of the

331   ASMA at all the pressure levels. The increase is quite significant at 100 hPa and even at 121 hPa.

332   The increase of O_3 is still appearing over the northeastern edges of the ASMA in August as

333   observed in July. Overall, a significant enhancement of O_3 within the ASMA is clear evidence in

334   July and August 2015.

335   The significant increase of O_3 within the ASMA in 2015 might be due to the transport from

336   the mid-latitudes through the STJ and also due to the stratosphere to the troposphere transport. For

337   example, the strong enhancement of O_3 within the ASMA at 100 hPa in July was strongly matched

338   with the observed high values of PV at 350 K isentropic surface (Fig. 6). This is further supported

339   by the strong southward meandering of STJ in July (Fig. 3), respectively. Thus, a clear transport

340   of mid-latitude air with high PV and high O_3 is evident during 2015. At the same time, the

341   enhancement of O_3 was clearly observed at all the pressure levels from 82 hPa to 121 hPa which

342   is further supported for the stratosphere to the troposphere transport. Note that 82 hPa can represent

343 the lower stratosphere and 121 hPa for the upper troposphere (Das et al., 2020). It can be noticed

344 that the ASMA is strongly associated with troposphere-stratosphere transport as well as

345 stratosphere-troposphere transport (Garny and Randel, 2016; Fan et al., 2017). Also, it is well

346 reported that the northern part of the ASMA is an active region for stratosphere-troposphere

347 transport processes (Sprenger et al., 2003; Škerlak et al., 2014).

348   Similarly, significant lowering of O_3, particularly at 100 hPa and 82 hPa is clearly noticed

349 over the tropics (Fig. 7). This is quite expected due to the enhanced tropical upwelling (bringing

350 poor O_3 air from troposphere) caused by the strong El Niño conditions in July and August 2015.

351 As mentioned in the previous sections, strong El Niño conditions are clearly evident in July and

352 August 2015 (Fig. 1). The observed strong negative O_3 anomalies over the tropics from the present

353 study are well matched with the previous studies (Randel et al., 2009; Diallo et al., 2018). From

354 the present results, it is very clear that there is a significant decrease over the tropics and the

355 increase over the mid-latitudes in 2015. These changes observed in the O_3 (decrease and increase)

356 are attributed due to the strengthening of the tropical upwelling and enhanced dowelling from the

357 shallow branch of the Brewer-Dobson circulation in the mid-latitudes due to the strong El Niño

358 conditions in 2015. Overall, it is concluded that initially, during July, the O_3 is transported into the

359 anticyclone from the northeastern edges of the ASMA region through the sub-tropical westerlies

360 and then it is isolated within the ASMA region. This is further supported by the southward

361 meandering of the westerly jet and southward shift of the ASMA (negative GPH anomalies) over

362 the same region in July (**Fig. 3**). Also, significant transport of mid-latitude dry air is clear from the

363 Fig. 6. Thus, it is clear from the results that the stratosphere to troposphere transport and horizontal

364 advection along with the subtropical jet caused the strong enhancement of the O_3 within the ASMA

365 in 2015.

Figure 8a-b (**Fig. 8c-d**) shows the spatial distribution of CO relative percentage change at 100 hPa and 146 hPa observed during July (August) 2015. The white (black) color contour represents 16.75 km GPH at 100 hPa for the corresponding month in 2015 (climatological mean). The observed changes in the CO clearly exhibit quite distinct features between July and August as observed in the O_3. A significant decrease (~30%) is noticed in the CO concentrations over most of the AMSA in July. The maximum decrease of CO is noticed over the northeastern edges of the ASMA, located ~ 30-45°N, 90-120°E region. Whereas in August, the decrease of CO is more concentrated over the east and western edges of the ASMA at both the pressure levels. Overall, the MLS observed CO was ~30% below average (percentage decrease) compared to the climatological monthly mean within the ASMA in July and edges of the ASMA in August 2015. It is noted that there is a considerable year-to-year variability of the CO sources over the ASM region (Santee et al., 2017). The major sources of the CO over the ASM region are from the biomass burning and industrial emission. The observed decreased CO within the ASMA in 2015 might be due to the year-to-year variability in the CO sources and the weaker vertical transport due to the El Niño conditions in 2015.

381
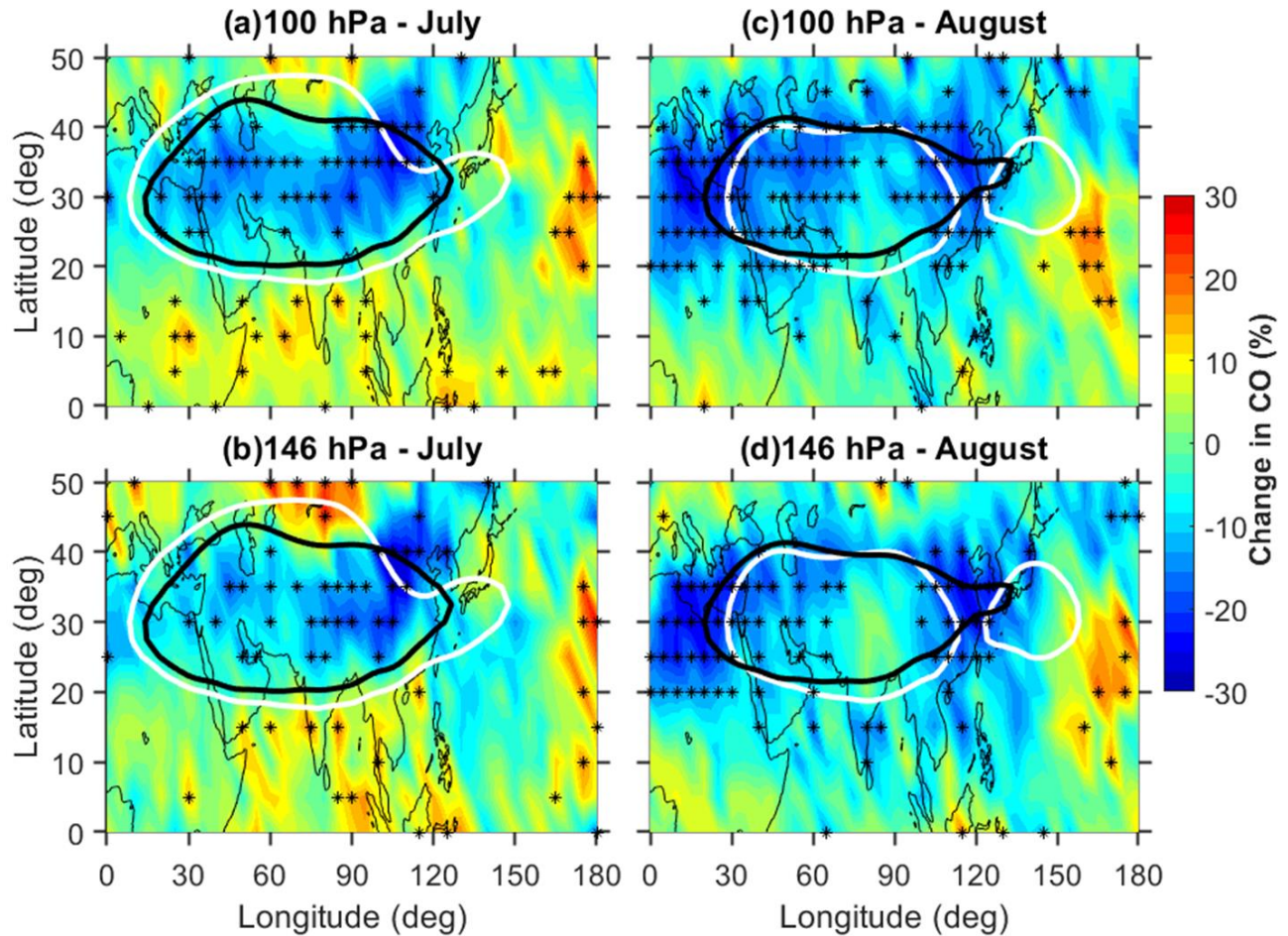
Figure 8. Carbon monoxide relative percentage change during July 2015 with respect to climatological monthly mean observed at (a) 100 hPa and (b) 146 hPa. Subplots of (c) and (d) same as (a) and (b) but for the month of August. The white (black) color contour represents 16.75 km geopotential height at 100 hPa for the corresponding month in 2015 (mean of 2005-2014). The star symbols (black) shown in figure represent the anomalies greater than the ±2σ standard deviation of long-term mean. The results are obtained from MLS measurements.

Similarly, the WV relative percentage change at 82 hPa, 100 hPa and 146 hPa in July (August) 2015 are shown in **Fig. 9a-c** (**Fig. 9d-f**). The WV shows quite different changes at all the pressure levels in July and August. At 146 hPa, the WV exhibits a strong decrease > 20%) within the ASMA in July as well as in August also. However, at 100 hPa and 82 hPa, the WV shows a relatively significant decrease within the ASMA in July compared to August. From the WV observations, it is concluded that the WV is strongly decreased at 146 hPa in both months. Whereas at 100 hPa

394 and 82 hPa, the decrease in WV is quite high in July compared to August. It is also observed from

395 the Fig. 9 that there is a significant enhancement of WV over the tropics at 146 hPa in both months.

396 But the WV enhancement is quite significant at 100 hPa, particularly during August compared to

397 July. This enhancement in the WV around the tropical tropopause region in August is quite

398 expected due to the El Niño conditions (Randel et al., 2009; Konopka et al., 2016). Overall, the

399 tropospheric tracers (CO and WV) significantly decreased (~30% and 20%) within the ASMA

400 during July and August 2015. These changes in the tropospheric tracers are might be due to the

401 weaker vertical motions during the 2015 monsoon. A weaker vertical transport from the boundary

402 layer to the UTLS is generally observed over the ASM region during El Niño period (Fadnavis et

403 al., 2019). The El Niño conditions will suppress the monsoon convection and cause weaker vertical

404 transport during monsoon. Also it is reported that the summer monsoon in 2015 was weaker

405 monsoon due to the strongest El Niño conditions existed in 2015 (Tweedy et al., 2018; Yuan et al.,

406 2019; Fadnavis et al., 2019).

407
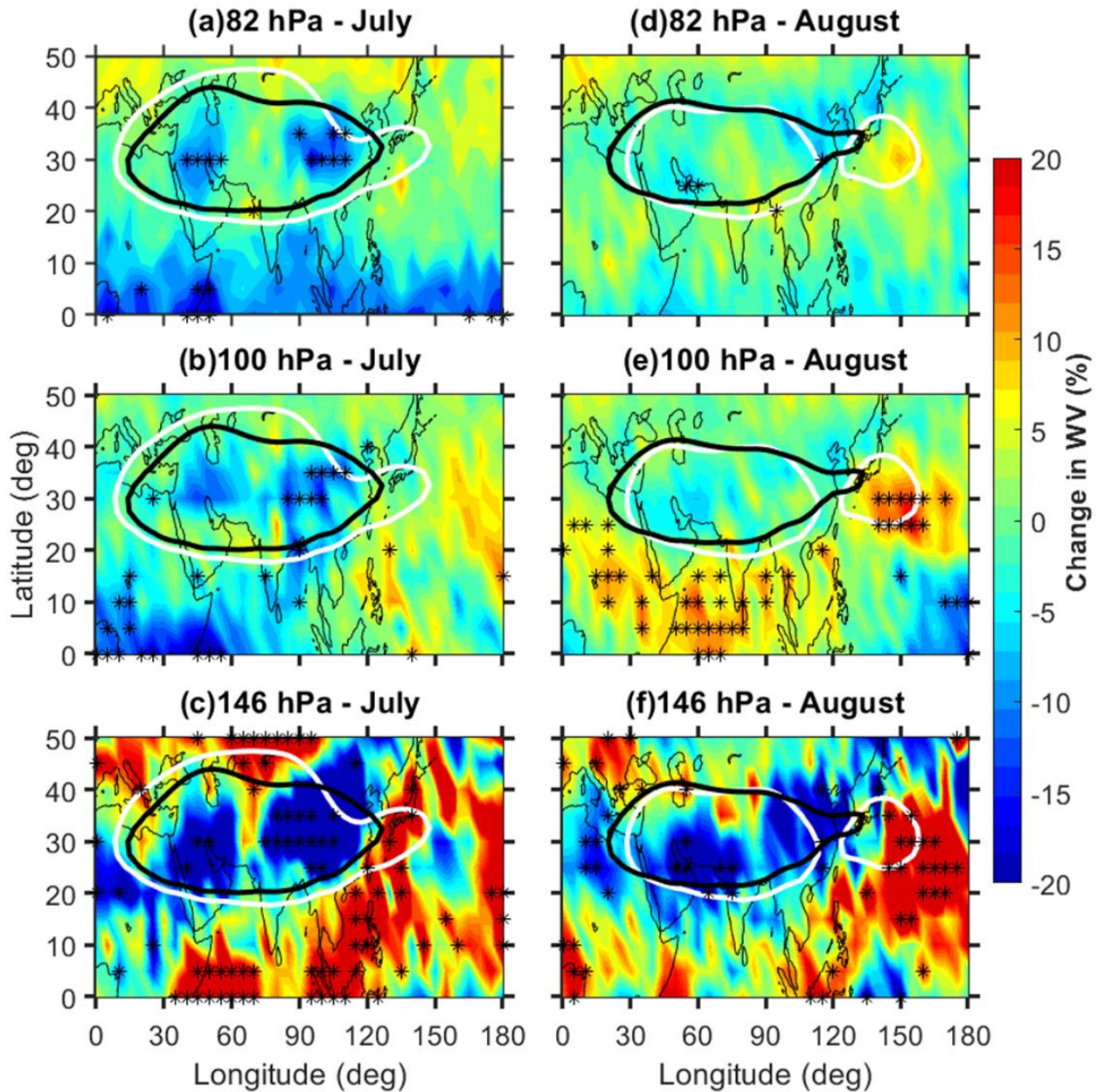
Figure 9. Water vapour relative percentage change in July 2015 with respect to background climatological monthly mean observed at (a) 82 hPa, (b) 100 hPa and (c) 146 hPa. Subplots of (d), (e) and (f) same as (a), (b) and (c) but for the month of August. The white (black) color contour represents 16.75 km geopotential height at 100 hPa for the corresponding month in 2015 (mean of 2005-2014). The star symbols (black) shown in figure represent the anomalies greater than the $\pm 2\sigma$ standard deviation of long-term mean. The results are obtained from MLS measurements.

From these results, it is clear that the enhancement of O_3 and lowering of CO/WV is evident in July and August 2015 compared to the long-term monthly mean. The observed high O_3 and low

416   WV within the ASMA from the present study are consistent and well-matched with the previous

417   study reported by Li et al. (2018). They demonstrated the importance of the large-scale

418   atmospheric dynamics and the stratospheric intrusions for high O_3 and low WV over Lhasa within

419   the ASMA by using in-situ balloon-borne measurements. The O_3/WV changes strongly influence

420   the background temperature structure within the UTLS region (Venkat Ratnam et al., 2016;

421   RavindraBabu et al., 2019b). Further, we investigated the tropopause temperature changes within

422   the ASMA by using COSMIC RO data. The results are presented in the next following section.

423   **3.3. Tropopause temperature anomalies in 2015**

424   It is well known that the tropopause plays a crucial role in the exchange of WV, O_3 and other

425   chemical species between the troposphere and the stratosphere. Most of these exchanges (WV to

426   the lower stratosphere and O_3 to the upper troposphere) known as stratosphere troposphere

427   exchange (STE) take place around the tropopause region (Fueglistaler et al., 2009; Venkat Ratnam

428   et al., 2016; RavindraBabu et al., 2019b). It is well reported that the tropopause within the ASMA

429   is higher than the outside regions at the same latitude (Randel et al., 2010; Santee et al., 2017). In

430   the present study, we mainly focused on changes in the cold point tropopause temperature (CPT)

431   and lapse rate tropopause temperature (LRT) within the ASMA in July and August 2015. The July

432   and August 2015 monthly mean tropopause parameters are removed from the respective

433   climatological monthly mean which is calculated by using COSMIC RO data from 2006 to 2014.

434   One can note that we have strictly restricted our analysis within 40ºN region for the cold point

435   tropopause. **Figure 10a-b** (**Fig. 10c-d**) shows the CPT and LRT anomalies observed in July

436   (August) 2015. The tropopause temperature anomalies (CPT/LRT) also exhibit a distinct pattern

437   in July and August as observed in O_3 (**Fig. 7**). In July, the CPT/LRT show strong positive anomalies

438   (~5 K) in most of the ASMA region. High positive CPT/LRT anomalies are also noticed over the

439   NWP region particularly below 20ºN. These CPT/LRT anomalies observed over the NWP region

440   might be due to the El Niño induced changes in the Walker circulation and convective activity.

441   Previous studies also observed significant warm tropopause temperature anomalies over WP and

442   maritime continent during the El Niño period (Gettleman et al., 2001). In August, the strong

443   positive CPT/LRT anomalies (~5K) are concentrated over the northeastern edges of the

444   anticyclone where the WP mode of the anticyclone was separated from the ASMA. The

445   temperature anomalies at 1 km above and below the CPH also show similar behavior as seen in

446   the CPT/LRT during August 2015 (figures not shown). Overall, the tropopause temperature

447   anomalies in July and August 2015 within the ASMA are well correlated with the strong

448   enhancement in the O_3 as shown in **Fig. 7.** However, the enhanced O_3 anomalies (heating due to

449   the O_3) itself cannot explain the observed positive tropopause temperature anomalies within the

450   ASMA in 2015. This might be due to the El Niño induced changes in the convective activity and

451   the circulation. It is well known that the reversal of walker circulation and the shifting of the

452   convective activity (suppressed convective activity over ASM region) are generally observed

453   during the warm phase of ENSO. One can be noticed that apart from the convection, other factors

454   such as stratospheric QBO, atmospheric waves (gravity waves and Kelvin waves) also strongly

455   influenced the tropopause temperatures.
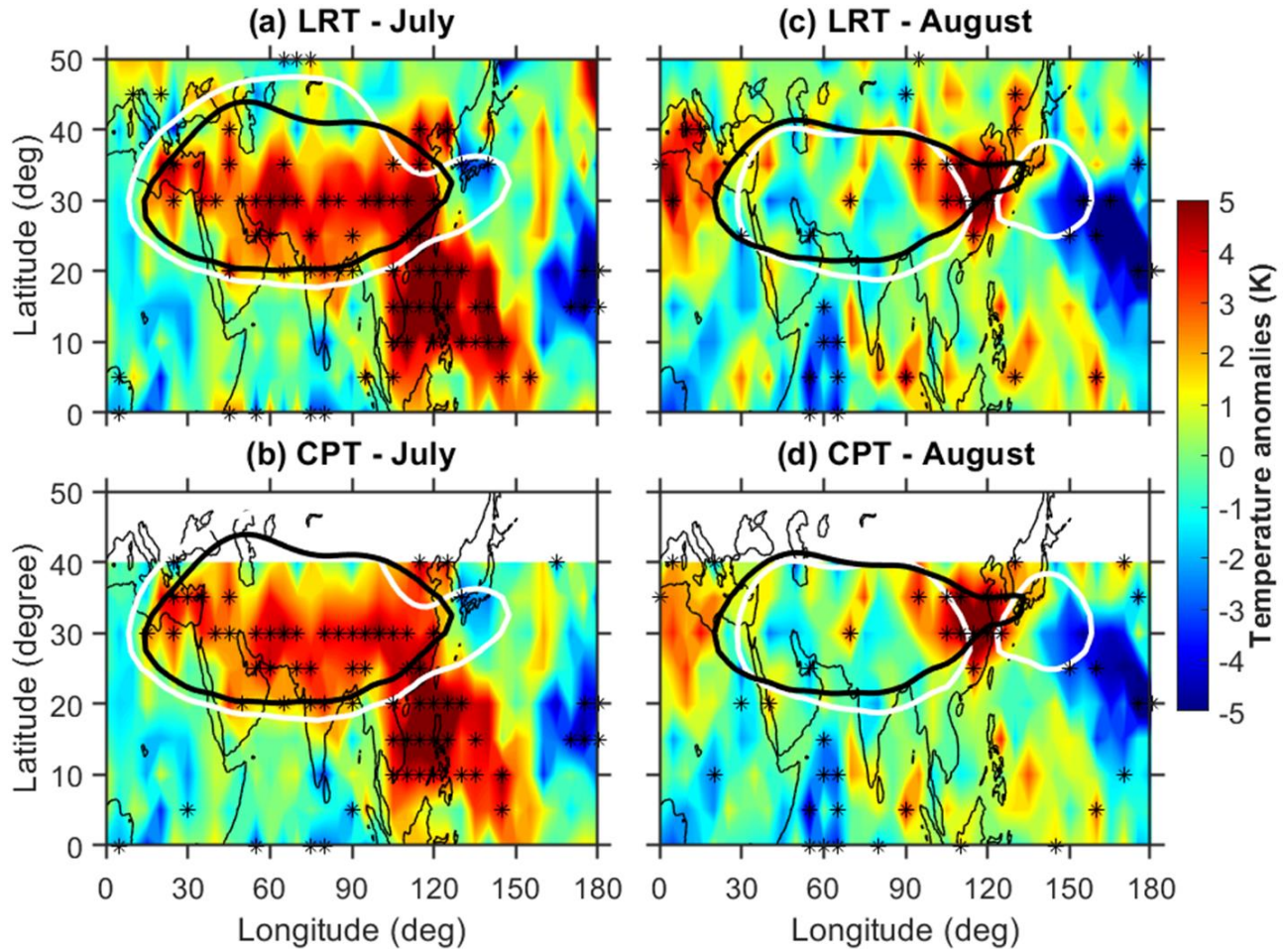
Figure 10. Spatial distribution of (a) lapse rate tropopause temperature (LRT), (b) cold point

tropopause temperature (CPT) anomalies during July 2015. Subplots of (c) and (d) same as (a) and

(b) but for the month of August 2015. The white (black) color contour represents 16.75 km

geopotential height at 100 hPa for the corresponding month in 2015 (mean of 2005-2014). The star

symbols (black) shown in figure represent the anomalies greater than the ±2σ standard deviation

of long-term mean.

4. Summary and Conclusions

In this study, we investigated the detailed changes observed in the structure, dynamics and

trace gases (Ozone, Water Vapor, Carbon Monoxide) variability within the ASMA in 2015 by using

reanalysis products and satellite observations. The tropopause temperature (CPT and LRT) on

467   monthly scales particularly during July and August 2015 also discussed. To quantify the changes

468   that happened within the ASMA region, 11 years (2005-2015) of O_3, WV and CO observations

469   from the Aura-MLS data and 10 years (2006-2015) of tropopause temperature data from the

470   COSMIC RO temperature profiles are used. The NCEP-DOE Reanalysis 2 observed winds and

471   GPH data from 2005 to 2015 are also utilized. The results are obtained by comparing the trace gas

472   quantities in July and August 2015 with corresponding long-term monthly mean quantities.

473   The trace gases within the ASMA exhibit substantial anomalous behavior in July and August

474   2015. During July and August 2015, we observed an enhancement of O_3 and the lowering of CO

475   and WV over most of the ASMA region. The decrease of the tropospheric tracers (CO and WV) is

476   quite expected due to the weaker upward motions from the weak monsoon in 2015. This is

477   supported by a recent study reported by Fadnavis et al. (2019). They showed weaker upward

478   motions and deficient rainfall in the 2015 monsoon due to the strong El Niño conditions. However,

479   the strong enhancement in the stratospheric tracer (O_3) within the ASMA particularly over the

480   northeastern edges of the ASMA during July is quite interesting. This is might be due to the

481   stratospheric intrusions as well as transport from the mid-latitudes. Based on Fishman and Seiler

482   (1983), it was stated that the positive correlation between CO and O_3 indicates, the O_3 is produced

483   by in-situ in the troposphere whereas the correlation is negative means the O_3 originates from the

484   stratosphere. We noticed a strong negative correlation between CO and O_3 in the present study

485   with increased O_3 and decreased CO from the MLS measurements. This clearly reveals that the

486   observed increased O_3 within the ASMA during 2015 is the stratospheric origin. This is further

487   supported by higher negative GPH anomalies associated with a southward meandering of the

488   subtropical westerly jet over northeastern Asia in July (**Figs. 3** and **4**). Further, the increased O_3 at

489   100 hPa and 121 hPa over western edges of the ASMA during August clearly indicates the transport

490 of the O_3 towards outer regions through the outflow of the ASMA (**Fig. 7e-f**). Interestingly, the

491 tropopause temperature obtained from the COSMIC RO data in July 2015 shows strong positive

492 temperature anomalies (~5 K) over the entire ASMA region. These warm tropopause temperatures

493 again supported the increased O_3 within the ASMA during 2015. The major findings obtained from

494 the present study are summarized in the following.

495 ❖ The spatial extension of the ASMA region shows higher than long-term mean except over

496   northeastern Asia where it exhibits a strong southward shift in July. Whereas in August, the

497   AMSA further separated into two anticyclones and the western Pacific mode anticyclone is

498   clearly evident in August.

499 ❖ The combination of Rossby wave breaking and pronounced southward meandering of

500   subtropical westerlies play a crucial role on the dynamical and structural changes in the

501   ASMA in 2015.

502 ❖ Strong enhancement in O_3 at 100 hPa (>40%) is clearly evident within the ASMA and

503   particularly higher over the northeastern edges of the ASMA in July. The enhanced O_3 is

504   strongly associated with a dominant southward meandering of the subtropical westerlies. In

505   August, the increased O_3 is significantly located over the western edges of the ASMA. This

506   clearly indicates the transport from the ASMA to the edges through its outflow.

507 ❖ A significant lowering of CO and WV within the ASMA is noticed during summer 2015. The

508   lowering of WV is higher at 146 hPa than 100 hPa.

509 ❖ Significant positive tropopause temperature anomalies (~5 K) is observed in the entire ASMA

510   region in July whereas, in August, the strong positive anomalies are concentrated over the

511   northeastern side of the ASMA.

512 The changes in the O_3 concentrations (increase/decrease) within the ASMA are one of the possible

513 mechanisms to strengthening/weakening of the ASMA (Braesicke et al., 2011). By using idealized

514 climate model experiments, Braesicke et al. (2011) clearly demonstrated that the strengthening

515 (weakening) of the ASMA occurred when the O_3 is decreased (increased) within the ASMA. The

516 increased O_3 within the ASMA warms the entire anticyclone region and weakens the ASMA

517 (Braesicke et al., 2011). Our results from the present study also in agreement with the results of

518 Braesicke et al. (2011). We also observed a pronounced increase of O_3 within the ASMA associated

519 with significant warming of tropopause as well as above and below the tropopause region in 2015.

520 By using precipitation index, wind data and stream functions, previous studies reported that the

521 ASMA circulation in 2015 was weaker than the normal (Tweedy et al., 2018; Yuan et al., 2019).

522 Based on our present results, the strongly enhanced O_3 within the ASMA also might be one of the

523 plausible reasons for weakening of the ASMA in 2015.

524 **Author contributions:** SRB designed the study, conducted research, performed initial data

525 analysis and wrote the first manuscript draft. MVR, GB, SKP and NHL edited the first manuscript.

526 All authors edited the paper.

527 **Data Availability:** All the data used in the present study is available freely from the respective

528 websites. The MLS trace gases data obtained from Earth Science Data website. The

529 NCEP_Reanalysis 2 data provided by the NOAA/OAR/ESRL PSL, Boulder, Colorado, USA, from

530 their web site (http://www.cpc.ncep.noaa.gov/products/wesley/reanalysis2/kana/reanl2-1.htm)

531 The COSMIC data is available from COSMIC CDAAC website (http://cdaac-

532 www.cosmic.ucar.edu/cdaac/products.html).

533 **Competing interests:** The authors declare that they have no conflict of interest.

534 **Acknowledgments:** Aura MLS observations obtained from the GES DISC through their FTP site

535 (https://mls.jpl.nasa.gov/index-eos-mls.php) is highly acknowledged. We thank the COSMIC Data

Analysis and Archive Centre (CDAAC) for providing RO data used in the present study through their FTP site (http://cdaac-www.cosmic.ucar.edu/cdaac/products.html). We also thank to NCEP/NCAR reanalysis for providing geopotential and wind data. We thank ECMWRF for providing ERA interim reanalysis data.

References

Anthes, R., Bernhardt, P., Chen, Y., Cucurull, L., Dymond, K., Ector, D., Healy, S., Ho, S., Hunt, D., Kuo, Y., Liu, H., Manning, K., Mccormick, C., Meehan, T., Randel, W., Rocken, C., Schreiner, W., Sokolovskiy, S., Syndergaard, S., Thompson, D., Trenberth, K., Wee, T., Yen, N., and Zeng, Z.: The COSMIC/FORMOSAT-3 – Mission early results, B. Am. Meteorol. Soc., 89, 313–333, 2008.

Avery, M. A., Davis, S. M., Rosenlof, K. H., Ye, H., Dessler, A. E., 2017. Large anomalies in lower stratospheric water vapour and ice during the 2015–2016 El Niño, Nat. Geosci., 10, 405–409, https://doi.org/10.1038/ngeo2961.

Basha, G., Ratnam, M. V., and Kishore, P.: Asian Summer Monsoon Anticyclone: Trends and Variability, Atmos. Chem. Phys. Discuss., https://doi.org/10.5194/acp-2019-668, in review, 2019.

Bergman, J. W., Fierli, F., Jensen, E. J., Honomichl, S., and Pan, L. L.: Boundary layer sources for the Asian anticyclone: Regional contributions to a vertical conduit, J. Geophys. Res.-Atmos., 118, 2560–2575, https://doi.org/10.1002/jgrd.50142, 2013.

Bian, J. C., Pan, L. L., Paulik, L., Vömel, H., and Chen, H. B.: In situ water vapor and ozone measurements in Lhasa and Kunming during the Asian summer monsoon, Geophys. Res. Lett., 39, L19808, https://doi.org/10.1029/2012GL052996, 2012.

Braesicke, P., O. J. Smith, P. Telford, and J. A. Pyle (2011), Ozone concentration changes in the Asian summer monsoon anticyclone and lower stratospheric water vapour: An idealised model study, Geophys. Res. Lett., 38, L03810, doi:10.1029/2010GL046228.

Diallo, M., Riese, M., Birner, T., Konopka, P., Müller, R., Hegglin, M. I., Santee, M. L., Baldwin, M., Legras, B., and Ploeger, F.: Response of stratospheric water vapor and ozone to the unusual timing of El Niño and the QBO disruption in 2015–2016, Atmos. Chem. Phys., 18, 13055–13073, https://doi.org/10.5194/acp-18-13055-2018, 2018.

565   Das, S.S., Suneeth, K.V., Ratnam, M.V., Girach, I. A., Das, S. K.: Upper tropospheric ozone
566   transport from the sub-tropics to tropics over the Indian region during Asian summer monsoon,
567   Clim Dyn., 52: 4567. https://doi.org/10.1007/s00382-018-4418-6, 2019.

568   Das, S., and Suneeth, K. V.: Seasonal and interannual variations of water vapor in the upper
569   troposphere and lower stratosphere over the Asian Summer Monsoon region- in perspective of
570   the tropopause and ocean-atmosphere interactions", Journal of Atmospheric and Solar-
571   Terrestrial Physics 201, 105244, doi:10.1016/j.jastp.2020.105244, 2020.

572   Dessler, A. E., Schoeberl, M. R., Wang, T., Davis, S. M., Rosenlof, K. H., and Vernier, J. P.:
573   Variations of stratospheric water vapor over the past three decades, J. Geophys. Res. Atmos.,
574   119, 12 588–12 598, doi:10.1002/2014JD021712, 2014.

575   Dunkerton, T. J.: The quasi-biennial oscillation of 2015–2016: Hiccup or death spiral? Geophys.
576   Res. Lett., 43, 10547–10552, https://doi.org/10.1002/2016GL070921, 2016.

577   Fadnavis, S. and Chattopadhyay, R.: Linkages of subtropical stratospheric intraseasonal intrusions
578   with Indian summer monsoon deficit rainfall, J. Climate, 30, 5083–5095,
579   https://doi.org/10.1175/JCLI-D-16-0463.1, 2017.

580   Fadnavis, S., Sabin, T.P., Roy, C. et al.: Elevated aerosol layer over South Asia worsens the Indian
581   droughts. Sci Rep 9, 10268, doi:10.1038/s41598-019-46704-9, 2019.

582   Fan, Q., Bian, J. and Pan, L. L.: Stratospheric entry point for upper-tropospheric air within the
583   Asian summer monsoon anticyclone, Sci. China Earth Sci., 60, 1685–
584   1693, https://doi.org/10.1007/s11430-016-9073-5, 2017.

585   Fishman, J., and Seiler, W.: Correlative nature of ozone and carbon monoxide in the troposphere
586   - Implications for the tropospheric ozone budget; J. Geophys. Res. 88,
587   https://doi.org/10.1029/JC088iC06p03662, 1983.

588   Fueglistaler, S., Dessler, A. E., Dunkerton, T. J., Folkins, I., Fu, Q., and Mote, P. W.: Tropical
589   Tropopause Layer, Rev. Geophys., 47, G1004+, https://doi.org/10.1029/2008RG000267, 2009.

590   Gadgil, S. and Francis, P. A.: El Niño and the Indian rainfall in June. Curr Sci 110:1010–1022,
591   2016.

592   Garny, H. and Randel, W. J.: Transport pathways from the Asian monsoon anticyclone to the
593   stratosphere, Atmos. Chem. Phys., 16, 2703–2718, https://doi.org/10.5194/acp-16-2703- 2016,
594   2016.

595   Gettelman, A., Randel, W. J., Massie, S., Wu, F.: El Niño as a natural experiment for studying the

tropical tropopause region, J. Clim., 14, 3375– 3392, 2001.

Gettelman, A., Kinnison, D. E., Dunkerton, T. J., and Brasseur, G. P.: Impact of monsoon circulations on the upper troposphere and lower stratosphere, J. Geophys. Res.-Atmos., 109, D22101, https://doi.org/10.1029/2004JD004878, 2004.

Highwood, E. J. and Hoskins, B. J.: The tropical tropopause, Q. J. Roy. Meteor. Soc., 124, 1579– 1604, https://doi.org/10.1002/qj.49712454911, 1998.

Ho, S.-P., Anthes, R. A., Ao, C.O., Healy, S., Horanyi, A., Hunt, D., Mannucci, A.J., Pedatella, N., Randel, W.J., Simmons, A., Steiner, A., Xie, F., Yue, X., Zeng., Z.: The COSMIC/FORMOSAT-3 radio occultation mission after 12 years: Accomplishments, remaining challenges, and potential impacts of COSMIC-2. Bull Amer Met Soc 100 online version: https://journals.ametsoc.org/doi/pdf/10.1175/BAMS-D-18-0290.1

Honomichl, S. B., and Pan, L. L.: Transport from the Asian summer monsoon anticyclone over the western Pacific. Journal of Geophysical Research: Atmospheres, 125, e2019JD032094. https://doi.org/10.1029/2019JD032094, 2020.

Hossaini, R., Chipperfield, M., Montzka, M. P., Rap, S. A., Dhomse, S., and Feng, W.: Efficiency of short-lived halogens at influencing climate through depletion of stratopsheric ozone, Nat. Geosci., 8, 186–190, https://doi.org/10.1038/ngeo2363, 2015.

Jiang, J.H., Su, H., Zhai, C., Wu, L., Minschwaner, K., Molod, A.M., Tompkins, A.M.: An assessment of upper troposphere and lower stratosphere water vapor in MERRA, MERRA2, and ECMWF reanalyses using Aura MLS observations. J. Geophys. Res. Atmos. 120, 11. https://doi.org/10.1002/2015JD023752, 468–11,485, 2015.

Kanamitsu, M., Ebisuzaki, W., Woollen, J., Yang, S.-K., Hnilo, J. J., Fiorino, M., and Potter, G. L.: NCEP-DOE AMIP-II Renalalysys (R-2), B. Am. Meteorol. Soc., 83, 1631–1643, https://doi.org/10.1175/BAMS-83-11-1631, 2002.

Khan, A., Jin, S.: Effect of gravity waves on the tropopause temperature, altitude and water vapor in Tibet from COSMIC GPS Radio Occultation observations, J. Atmos. Sol. Terr. Phys. 138– 139, 23–31. https://doi.org/10.1016/j.jastp.2015.12.001, 2016.

Kim, J. and Son, S.-W.: Tropical Cold-Point Tropopause: Climatology, Seasonal Cycle, and Intraseasonal Variability Derived from COSMIC GPS Radio Occultation Measurements, J. Climate, 25, 5343–5360, https://doi.org/10.1175/JCLI-D-11-00554.1, 2012.

626 Kumar, K. K., Rajagopalan, B., Cane, M. A.: On the weakening relationship between the Indian
627   monsoon and ENSO. Science 287:2156–2159, 1999.

628 Kursinski, E. R., Hajj, G. A., Schofield, J. T., Linfield, R. P., and Hardy, K. R.: Observing Earth's
629   atmosphere with radio occultation measurements using the Global Positioning System, J.
630   Geophys. Res., 102, 23429–23465, 1997.

631 Konopka, P., Ploeger, F., Tao, M., and Riese, M.: Zonally resolved impact of ENSO on the
632   stratospheric circulation and water vapor entry values, J. Geophys. Res.-Atmos., 121, 11486–
633   11501, https://doi.org/10.1002/2015JD024698, 2016.

634 Li, Q., Jiang, J. H., Wu, D. L., Read, W. G., Livesey, N. J., Waters, J. W., Zhang, Y., Wang,B.,
635   Filipiak, M. J., Davis, C. P., Turquety, S., Wu, S., Park, R. J., Yantosca, R. M., and Jacob, D.
636   J.: Convective outflow of South Asian pollution: A global CTM simulation compared with EOS
637   MLS observations, Geophys. Res. Lett., 32, L14 826, https://doi.org/10.1029/2005GL022762,
638   2005.

639 Li, D., Vogel, B., Müller, R., Bian, J., Günther, G., Li, Q., Zhang, J., Bai, Z., Vömel, H., and Riese,
640   M.: High tropospheric ozone in Lhasa within the Asian summer monsoon anticyclone in 2013:
641   influence of convective transport and stratospheric intrusions, Atmospheric Chemistry and
642   Physics, 18, 17 979–17 994, https://doi.org/10.5194/acp-18-17979-2018, https://www.atmos-
643   chem-phys.net/18/17979/2018/, 2018.

644 Livesey, N. J., Read, W. G., Wagner, P. A., Froidevaux, L., Lambert, A., Manney, G. L., Valle, L.
645   F. M., Pumphrey, H. C., Santee, M. L., Schwartz, M. J., Wang, S., Fuller, R. A., Jarnot, R. F.,
646   Knosp, B. W., and Martinez, E.: Version 4.2x Level 2 data quality and description document,
647   https://mls.jpl.nasa.gov/data/v4-2_data_quality_document.pdf, 2018

648 Nützel, M., Dameris, M., and Garny, H.: Movement, drivers and bimodality of the South Asian
649   High, Atmos. Chem. Phys., 16, 14755–14774, https://doi.org/10.5194/acp-16-14755-2016,
650   2016.

651 Pan, L. L., Honomichl, S. B., Kinnison, D. E., Abalos, M., Randel, W. J., Bergman, J. W., and
652   Bian, J. C.: Transport of chemical tracers from the boundary layer to stratosphere associated
653   with the dynamics of the Asian summer monsoon, J. Geophys. Res.-Atmos., 121, 14159–14174,
654   https://doi.org/10.1002/2016JD025616, 2016.

655 Park, M., Randel, W. J., Kinnison, D. E., Garcia, R. R., and Choi, W.: Seasonal variation of
656   methane, water vapor, and nitrogen oxides near the tropopause: Satellite observations and

657   model simulations, J. Geophys. Res.-Atmos., 109, D03302,
658   https://doi.org/10.1029/2003jd003706, 2004.

659   Park, M., Randel, W. J., Gettelman, A., Massie, S. T., and Jiang, J. H.: Transport above the Asian
660   summer monsoon anticyclone inferred from Aura MLS tracers, J. Geophys. Res, 112, D16309,
661   doi:10.1029/2006JD008294, 2007.

662   Park, M., Randel, W. J., Emmons, L. K., Bernath, P. F., Walker, K. A., and Boone, C. D.: Chemical
663   isolation in the Asian monsoon anticyclone observed in Atmospheric Chemistry Experiment
664   (ACE-FTS) data, Atmos. Chem. Phys., 8, 757–764, https://doi.org/10.5194/acp-8-757-2008,
665   2008

666   Park, M., Randel, W. J., Emmons, L. K., and Livesey, N. J.: Transport pathways of carbon
667   monoxide in the Asian summer monsoon diagnosed from Model of Ozone and Related Tracers
668   (MOZART), J. Geophys. Res., 114, D08303, https://doi.org/10.1029/2008JD010621, 2009.

669   Ramaswamy, C.: A preliminary study of the behavior of the Indian southwest monsoon in relation
670   to the westerly jet-stream. Special Palmen No. Geophysica, 6, pp. 455-476, 1958.

671   Randel, W. J. and Park, M.: Deep convective influence on the Asian summer monsoon anticyclone
672   and associated tracer variability observed with Atmospheric Infrared Sounder (AIRS), J.
673   Geophys. Res., 111, D12314, https://doi.org/10.1029/2005jd006490, 2006.

674   Randel, W. J., Garcia, R. R., Calvo, N., and Marsh, D.: ENSO influence on zonal mean temperature
675   and ozone in the tropical lower stratosphere, Geophys. Res. Lett., 36, L15822,
676   https://doi.org/10.1029/2009GL039343, 2009.

677   Randel, W. J., Park, M., Emmons, L., Kinnison, D., Bernath, P., Walker, K. A., Boone, C., and
678   Pumphrey, H.: Asian Monsoon Transport of Pollution to the Stratosphere, Science, 328, 611–
679   613, https://doi.org/10.1126/science.1182274, 2010.

680   Rao, D.N., Ratnam, M.V., Mehta, S., Nath, D., Basha, G., Jagannadha Rao, V.V.M., et al:
681   Validation of the COSMIC radio occultation data over gadanki (13. 48°N, 79.2°E): A tropical
682   region, Terr J Atmos Ocean Sci 20, 59–70, https://doi.org/10.3319/TAO.2008.01.23.01(F3C),
683   2009.

684   RavindraBabu, S., VenkatRatnam, M., Basha, G., Krishnamurthy, B. V., and Venkateswararao, B.:
685   Effect of tropical cyclones on the tropical tropopause parameters observed using COSMIC GPS
686   RO data, Atmos. Chem. Phys., 15, 10239–10249, doi:10.5194/acp-15-10239-2015, 2015.

RavindraBabu, S., VenkataRatnam, M., Basha, G., Liou, Y.-A., Narendra Reddy, N.: Large Anomalies in the Tropical Upper Troposphere Lower Stratosphere (UTLS) Trace Gases Observed during the Extreme 2015–16 El Niño Event by Using Satellite Measurements, Remote Sensing. 2019, 11, 687.https://doi.org/10.3390/rs11060687, 2019. a

RavindraBabu, S., Venkat Ratnam, M., Basha, G., Krishnamurthy, B.V.: Indian summer monsoon onset signatures on the tropical tropopause layer. Atmos. Sci. Lett. 20, e884. https://doi.org/10.1002/asl.884, 2019. b

Ravindra Babu, S., Akhil Raj, S.T., Basha, G., Venkat Ratnam, M.: Recent trends in the UTLS temperature and tropical tropopause parameters over tropical South Indian region, J. Atmos. Solar Terr. Phys. 197:105164. https://doi.org/10.1016/j.jastp.2019.105164, 2020.

Ravindra Babu, S. and Liou, Y. A.: Tropical tropopause layer evolution during 2015–16 El Niño event inferred from COSMIC RO measurements, J. Atmos. Solar Terr. Phys. 212: 105507. https://doi.org/10.1016/j.jastp.2020.105507

Samanta, D., Dash, M. K., Goswami, B. N., and Pandey, P. C.: Extratropical anticyclonic Rossby wave breaking and Indian summer monsoon failure. Climate Dyn., 46, 1547–1562, doi:https://doi.org/10.1007/s00382-015-2661-7., 2016.

Santee, M. L., Manney, G. L., Livesey, N. J., Schwartz, M. J., Neu, J. L., and Read, W. G.: A comprehensive overview of the climatological composition of the Asian summer monsoon anticyclone based on 10 years of Aura Microwave Limb Sounder measurements, J. Geophys. Res.-Atmos., 122, 5491- 5514, https://doi.org/10.1002/2016jd026408, 2017.

Scherllin-Pirscher, B., Kirchengast, G., Steiner, A. K., Kuo, Y.-H., and Foelsche, U.: Quantifying uncertainty in climatological fields from GPS radio occultation: an empirical-analytical error model, Atmos. Meas. Tech., 4, 2019–2034, doi:10.5194/amt-4-2019-2011, 2011a.

Scherllin-Pirscher, B., Steiner, A. K., Kirchengast, G., Kuo, Y.-H., and Foelsche, U.: Empirical analysis and modeling of errors of atmospheric profiles from GPS radio occultation, Atmos. Meas. Tech., 4, 1875–1890, doi:10.5194/amt-4-1875-2011, 2011b.

Sprenger, M., Maspoli, M. C., and Wernli, H.: Tropopause folds and cross-tropopause exchange: A global investigation based upon ECMWF analyses for the time period March 2000 to February 2001, J. Geophys. Res., 108, 8518, https://doi.org/10.1029/2002JD002587, 2003.

Škerlak, B., Sprenger, M., and Wernli, H.: A global climatology of stratosphere–troposphere exchange using the ERA-Interim data set from 1979 to 2011, Atmos. Chem. Phys., 14, 913–937, https://doi.org/10.5194/acp-14-913-2014, 2014.

Tweedy, O. V., Waugh, D. W., Randel, W. J., Abalos, M., Oman, L. D., and Kinnison, D. E.: The Impact of Boreal Summer ENSO Events on Tropical Lower Stratospheric Ozone, Journal of Geophysical Research: Atmospheres, 123, 9843–9857, https://doi.org/10.1029/2018JD029020.

Uppala, S. M., Kållberg, P. W., Simmons, A. J., Andrae, U., da Costa Bechtold, V., Fiorino, M., Gibson, J. K., Haseler, J., Hernandez, A., Kelly, G. A., Li, X., Onogi, K., Saarinen, S., Sokka, N., Allan, R. P., Andersson, E., Arpe, K., Balmaseda, M. A., Beljaars, A. C. M., van de Berg, L., Bidlot, J., Bormann, N., Caires, S., Chevallier, F., Dethof, A., Dragosavac, M., Fisher, M., Fuentes, M., Hagemann, S., Hólm, E., Hoskins, B. J., Isaksen, L., Janssen, P. A. E. M., Jenne, R., McNally, A. P., Mahfouf, J. F., Morcrette, J. J., Rayner, N. A., Saunders, R. W., Simon, P., Sterl, A., Trenberth, K. E., Untch, A., Vasiljevic, D., Viterbo, P., and Woollen, J.: The ERA-40 re-analysis, Q. J. Roy. Meteor. Soc., 131, 2961–3012, https://doi.org/10.1256/qj.04.176, 2005.

Vellore, R. K., Kaplan, M. L., and Krishnan, R., et al.: Monsoon-extratropical circulation interactions in Himalayan extreme rainfall; *Clim. Dyn.* **46,** 3517, 2016. https://doi.org/10.1007/s00382-015-2784-x.

Venkat Ratnam, M., Ravindra Babu, S., Das, S. S., Basha, G., Krishnamurthy, B. V., and Venkateswararao, B.: Effect of tropical cyclones on the stratosphere–troposphere exchange observed using satellite observations over the north Indian Ocean, Atmos. Chem. Phys., 16, 8581–8591, https://doi.org/10.5194/acp-16-8581-2016, 2016.

Vernier, J.-P., Thomason, L. W., and Kar, J.: CALIPSO detection of an Asian tropopause aerosol layer, Geophys. Res. Lett., 38, L07804, https://doi.org/10.1029/2010GL046614, 2011

Vernier, J.-P., Fairlie, T. D., Deshler, T., Ratnam, M. V., Gadhavi, H., Kumar, B. S., Natarajan, M., Pandit, A. K., Raj, S. T. A., Kumar, A. H., Jayaraman, A., Singh, A. K., Rastogi, N., Sinha, P. R., Kumar, S., Tiwari, S., Wegner, T., Baker, N., Vignelles, D., Stenchikov, G., Shevchenko, I., Smith, J., Bedka, K., Kesarkar, A., Singh, V., Bhate, J., Ravikiran, V., Rao, M. D., Ravindrababu, S., Patel, A., Vernier, H., Wienhold, F. G., Liu, H., Knepp, T. N., Thomason, L., Crawford, J., Ziemba, L., Moore, J., Crumeyrolle, S., Williamson, M., Berthet, G., Jégou, F., and Renard, J.- B.: BATAL: The balloon measurement campaigns of the Asian tropopause

aerosol layer, B. Am. Meteorol. Soc., 99, 955–973, https://doi.org/10.1175/BAMS-D-17-0014.1, 2018.

Vogel, B., Günther, G., Müller, R., Grooß, J.-U., Afchine, A., Bozem, H., Hoor, P., Krämer, M., Müller, S., Riese, M., Rolf, C., Spelten, N., Stiller, G. P., Ungermann, J., and Zahn, A.: Longrange transport pathways of tropospheric source gases originating in Asia into the northern lower stratosphere during the Asian monsoon season 2012, Atmos. Chem. Phys., 16, 15301–15325, https://doi.org/10.5194/acp-16-15301-2016, 2016.

Wang, B., Xiang, B., Li, J., Webster, P. J., Rajeevan, M. N., Liu, J., Ha, K. –J.: Rethinking Indian monsoon rainfall prediction in the context of recent global warming. Nat Commun 6:7154. doi:10.1038/ncomms8154, 2015.

Xu, X., Zhao, T., Lu, C., Guo, Y., Chen, B., Liu, R., Li, Y., Shi, X.: An important mechanism sustaining the atmospheric "water tower" over the Tibetan Plateau. Atmos. Chem. Phys. 14, 11287–11295. https://doi.org/10.5194/acp-14-11287- 2014.

Yan, R.-C., Bian, J.-C., and Fan, Q.-J.: The Impact of the South Asia High Bimodality on the Chemical Composition of the Upper Troposphere and Lower Stratosphere, Atmos. Ocean. Sci. Lett., 4, 229–234, 2011.

Yan, R. C. and Bian, J. C.: Tracing the boundary layer sources of carbon monoxide in the Asian summer monsoon anticyclone using WRF–Chem, Adv. Atmos. Sci., 32, 943–951, https://doi.org/10.1007/s00376-014-4130-3, 2015.

Yan, X., Konopka, P., Ploeger, F., Tao, M., Müller, R., Santee, M. L., Bian, J., and Riese, M.: El Niño Southern Oscillation influence on the Asian summer monsoon anticyclone, Atmospheric Chemistry and Physics, pp. 8079–8096, https://doi.org/10.5194/acp-18-8079-2018, 2018.

Yu, P., Rosenlof, K. H., Liu, S., Telg, H., Thornberry, T. D., Rollins, A. W., Portmann, R. W., Bai, Z., Ray, E. A., Duan, Y., Pan, L. L., Toon, O. B., Bian, J., and Gao, R.-S.: Efficient transport of tropospheric aerosol into the stratosphere via the Asian summer monsoon anticyclone, Proceedings of the National Academy of Sciences, pp. 6972–6977, https://doi.org/10.1073/pnas.1701170114, 2017.

Yuan, C., Lau, W. K. M., Li, Z., and Cribb, M.: Relationship between Asian monsoon strength and transport of surface aerosols to the Asian Tropopause Aerosol Layer (ATAL): interannual variability and decadal changes, Atmos. Chem. Phys., 19, 1901-1913, https://doi.org/10.5194/acp-19-1901-2019, 2019.